Concerted effects of local and nonlocal plasmons on the broadband nonlinear optical response in tip-enhanced nanophotonics

Shota Takahashi[1], Atsunori Sakurai[1,2], Tatsuto Mochizuki[1,2], and Toshiki Sugimoto[1,2,3*]*

[1]Department of Materials Molecular Science, Institute for Molecular Science (IMS), Okazaki, Aichi 444-8585, Japan

[2]The Graduate University for Advanced Studies, SOKENDAI, Hayama, Kanagawa, 240-0193, Japan

[3]Precursory Research for Embryonic Science and Technology (PRESTO), Japan Science and Technology Agency (JST), 4-1-8 Honcho, Kawaguchi, Saitama 332-0012, Japan

KEYWORDS: tip-enhanced second harmonic generation, near-field optics, plasmonic nanocavity, nonlinear nanophotonics, plasmonics

*Corresponding authors

E-mail: asakurai@ims.ac.jp, toshiki-sugimoto@ims.ac.jp

ABSTRACT: We report critical impacts of local and nonlocal geometries of plasmonic tips on the broadband nonlinear optical responses in tip-substrate nanocavities. Using gold tips with varied geometries, we demonstrated for the first time that not only the nanometer-scale sharpness of tip apexes but also the micrometer-scale geometry of tip shafts directly affects the enhancement properties of second-harmonic generation over the visible-to-infrared wavelength range. Numerical simulations of the tip-substrate plasmonic field revealed concerted contributions from spatially nonlocal and local plasmonic modes. Micrometer-scale tip shafts enable the excitation of nonlocal plasmonic modes throughout the tip, enhancing near-to-mid-infrared incoming light. Subsequent radiation of visible-to-near-infrared second harmonics is boosted by localized plasmons at the nanogap. Based on the agreement between experiments and calculations, our results indicate the importance of nanometer- and micrometer-scale geometrical engineering of plasmonic tips and provide a firm basis to understand and finely manipulate nonlinear optical phenomena in tip-substrate nanocavities.

Light confined by tip-substrate plasmonic nanocavities provides site-specific information on physical properties at the molecular/atomic scale. When combined with scanning probe microscopy, the outstanding ability of nanocavities to shrink light beyond the diffraction limit renders them highly attractive for nanoscale photonics. In recent decades, a considerable number of studies have been conducted using this tip enhancement technique. Although linear optical responses (e.g., light scattering[1,2] and photoluminescence[3,4]) are a major focus in this field, several meaningful attempts at nanoscale detection of nonlinear optical processes have been made in recent years.[5] Sufficient sensitivity and spatial resolution have been demonstrated for second-harmonic generation,[6–12] sum-frequency generation,[7,11] coherent anti-Stokes Raman scattering,[13–16] and nonlinear four-wave mixing.[11,17,18] Further development of such tip-enhanced nonlinear optical techniques will promote a deeper understanding of correlated chemical and topographic information with ultimate spatial and temporal resolution.

The manipulation of tip-enhanced nonlinear optical effects and their application to the spectroscopic analysis of materials requires a fundamental understanding of the nonlinear optical properties of tip-substrate nanocavities. Particularly, the optical wavelength range over which tip enhancement works effectively must be considered. Nonlinear optical processes are often accompanied by drastic frequency conversion between incoming and outgoing light. Therefore, a spectrally broad plasmonic enhancement that can simultaneously affect such separated frequencies is required to efficiently enhance nonlinear optical phenomena.[19–21] Characterizing and exploiting the operating wavelength range of field enhancement is therefore essential for controlling nonlinear optical processes in tip-substrate nanocavities.

Despite such fundamental importance, there has been no conclusive studies on broadband nonlinear optical responses in tip-substrate nanogaps. Although most studies have given basic demonstration of tip-enhanced nonlinear optics as a nanoscale spatial imaging technique, little effort has been devoted to characterizing the optical properties of tip-substrate nanocavities in the spectral domain. Recently, tip-enhanced second-harmonic generation (TESHG) in the visible-to-infrared range was investigated for specific 2D semicondutors.[12] However, owing to the exciton absorption, the excitonic resonance enhancement dominated the observed spectral features of TESHG. Therefore, the plasmonic nonlinear optical responses intrinsic to the tip-substrate nanocavities in the broad wavelength range remain to be fully understood.

In this Letter, we for the first time investigate the inherent SHG response of a tip-substrate nanocavity over a visible-to-infrared broad wavelength range of 650–2000 nm. By performing systematic experiments using tips with different geometries and a metallic substrate free from electronic resonance effects, we found that not only the nanometer-scale but also the micrometer-scale structure of tips has significant impact on the nonlinear optical responses in the nanogap over a broad wavelength range. Based on finite-difference time-domain (FDTD) simulations of plasmonic fields incorporating realistic tip geometries, we reveal that this geometrical effect of the tips is closely related to two types of plasmonic modes with distinct spatial scales. Micrometer-scale tip shafts play critical roles in trapping and enhancing infrared excitation pulses through supporting collective oscillation of electrons throughout the tip, which can be regarded as nonlocal plasmonic modes. Subsequently, localized nanosized plasmons excited at the nanoscale tip apexes predominantly boost the radiation of second-harmonics in the visible range. These micrometer- and nanometer-scale geometrical effects of the tips jointly enable the enhancement of the nonlinear optical processes encompassing the visible-to-infrared broadband spectral region.

Figure 1a shows the experimental setup. To form a tip-substrate nanocavity, we employed a scanning tunneling microscope (STM) unit placed inside a UHV chamber (UNISOKU, USM1400SA-TL01). The second-order nonlinear optical signal was generated by irradiating a tip-substrate nanocavity with infrared excitation pulses (300 fs) at a high repetition rate (50 MHz). Plasmonic STM tips were fabricated by electrochemically etching gold wires. Typical scanning electron micrographs of a fabricated tip are shown in Figures 1b and c. We denote this tip as tip #1 for later discussion. Note that based on previous work,[22] we can reproducibly fabricate tips with smooth shafts, minimal roughness, and apexes with sub-micron scale curvature radii, as shown in Figures 1b and c.

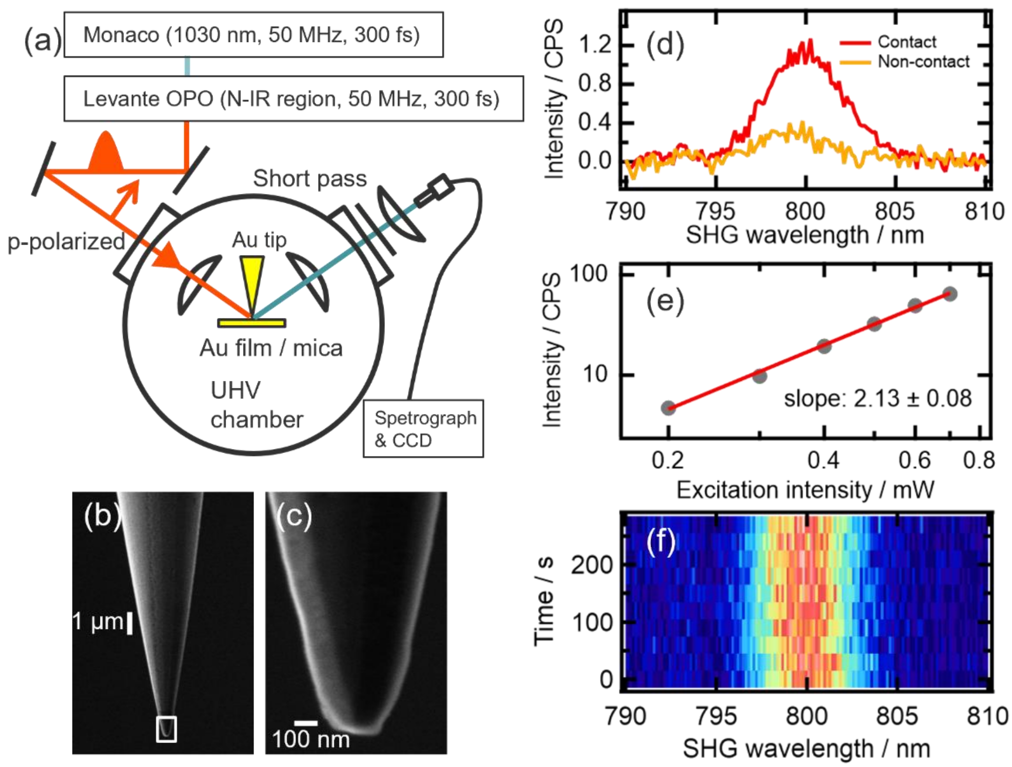

Figure 1. (a) Schematic representation of our experimental setup for TESHG measurement. (b) Scanning electron micrograph of the Au tip. (c) Zoomed-in view of the white square region in (b). (d) Spectrally resolved SHG signals obtained with (red) and without (orange) tunneling contact. (e) A logarithmic plot of the excitation power dependence of the spectrally integrated TESHG intensity (gray filled circles). The red line represents a power fit to the corresponding data points. (f) Time series of TESHG spectra measured consecutively with an excitation power of 0.7 mW. The acquisition time for each spectrum was 30 s.

We chose an atomically flat, clean Au(111) surface with wide terraces as a substrate to form a nanogap. Nanocavities formed between well-defined smooth gold tips and a substrate are suitable platforms for investigating the intrinsic nonlinear optical response of nanocavities, free from the influence of electronic resonances. The edge of the interband transition of bulk gold (5d → 6sp) is located at around 2.3 eV (539 nm),[23] below which no appreciable electronic transitions of the bulk exist. Moreover, previous studies on scanning tunneling spectroscopy for clean gold substrates[24–26] confirmed that gold possesses no surface states below 3.5 eV (longer than 354 nm). Owing to the absence of such surface states or bulk electronic transitions in a certain energy range, we are able to disregard the large electronic-resonance-assisted optical enhancement effects by carefully choosing the range of the excitation—and hence radiation—wavelength. In this context, the center wavelength of incident pulses was scanned from 1300 nm to 2000 nm, resulting in SHG output between 650 nm and 1000 nm. These wavelengths are off-resonant with the inherent electronic transitions of gold; we can therefore focus on the intrinsic nonlinear optical responses in the tip-substrate nanocavity.

Signals were recorded when (i) the tip and the substrate were in tunneling contact regime and (ii) the tip-substrate distance was elongated by 30 nm. Note that the signals obtained in situation (ii) correspond to far-field SHG without plasmonic enhancement effects. Figure 1d shows the typical SHG spectra for these two situations. The SHG intensity increased in the tunneling contact regime. This is because the optical enhancement effect was present when a plasmonic nanocavity was formed between the substrate and the apex of the tip. In all experimental results shown below, the far-field signals obtained in situation (ii) were subtracted from the signals in situation (i), which contained both near- and far-field contributions. This allowed us to focus on a pure near-field signal.

Signal stability in tip-enhanced nanophotonics is vulnerable to the atomistic structural fluctuations of a plasmonic nanocavity.[27] Such fluctuations can be promoted by the excessive peak power density of excitation pulses.[28,29] To perform stable experiments, the threshold of the excitation intensity above which signals become unstable must be carefully ascertained. Considering this, we measured TESHG intensity by varying the excitation power (Figure 1e).

Below 0.8 mW, the intensity of the TESHG signal scaled quadratically, as is generally expected for second-order nonlinear optical processes. Within this power range, the TESHG intensity remained almost constant for over 300 s (Figure 1f). In contrast, when the power was increased to 1 mW, the TESHG intensity started to fluctuate and deviated from the quadratic dependence (Figure S1). These results indicate that as long as the excitation power is kept sufficiently low (≤ 0.7 mW), the output of TESHG signal is stable without any appreciable signal fluctuations.

To investigate the spectral properties of the TESHG, we tuned the center wavelength of the incident pulses and monitored the variation in the TESHG spectra. The excitation intensity was kept low and constant (0.3 mW) over the entire swept-wavelength range. Figure 2 shows a series of TESHG spectra and their peak-top intensities measured at various excitation wavelengths using the tip #1 shown in Figures 1b and c. TESHG output was observed over an excitation wavelength

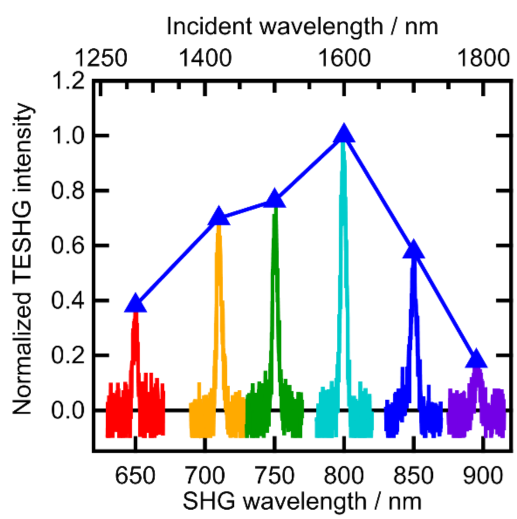

Figure 2 (Colored spectra) TESHG spectra obtained by tuning the center wavelength of incident pulses. (Blue triangles) Variation of the TESHG intensities at the peak-top of the individual spectra. All data in the figure are normalized by the peak-top value obtained when the excitation wavelength is 1600 nm and plotted as a function of SHG wavelengths (bottom axis) and corresponding incident beam wavelengths (top axis).

of several hundred nanometers. Because the scanned wavelength range is detuned from any electronic transitions of gold, the wavelength dependence of the second-order nonlinear susceptibility ($\chi^{(2)}$) of gold should be small. Hence, the observed dependence is considered to originate from other factors not discussed yet.

Additional experiments using gold tips with different structures showed that the nonlinear optical properties of nanogaps are highly influenced by tip geometry. To demonstrate this, we fabricated a gold tip (tip #2) with a macroscopic shaft shape similar to that of tip #1 but a sharper tip apex (Figures 1b and c), as shown in Figures 3a and b. The intensity of TESHG from this tip sharply declined with an increase in the input infrared wavelength, as shown in Figure 3c, which

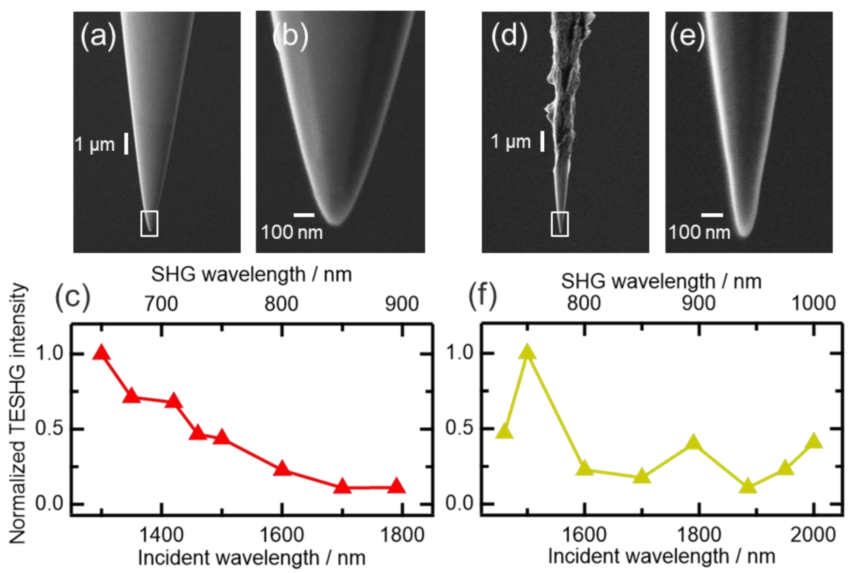

Figure 3. Scanning electron micrographs of (a, b) tip #2 and (d, e) #3. Zoomed-in views of white square regions in (a) and (d) are shown in (b) and (e), respectively. (c, f) The intensities of TESHG obtained for (c) tip #2 and (f) #3. Data are normalized by their maximum values and plotted as a function of the center wavelengths of the incident beams (bottom axis) and corresponding SHG wavelengths (top axis).

is in stark contrast to the result for tip #1 (Figure 2). These results clearly indicate the critical importance of nanoscale tip sharpness for plasmonic nonlinear optical properties.

In addition to the nanometer-scale tip apexes, micrometer-scale structure of the tip shafts also has a significant impact on nonlinear optical responses from tip-substrate nanocavities. As shown in Figure 3f, the tip with micrometer-scale surface roughness introduced on the shaft (tip #3, Figure 3d) exhibited drastically distinct nonlinear optical behavior. Although the surface around the apex of tip #3 was smooth (Figure 3e) and the bumps on the shaft were separated from the apex by as much as ~3 μm, a multimodal structure emerged in the spectral profile of the TESHG from the nanogap (Figure 3f). This indicates that in addition to the nanometer-scale curvature of the tip apex, the micrometer-scale surface geometry of the shaft also determines the spectral properties of SHG enhancement inside nanocavities. The dependence on tip geometry suggests the existence of two different plasmonic effects: spatially local effects that occur at nanometer-scale tip apexes and nonlocal effects governed by micrometer-scale tip shafts.

To gain detailed insights into these local and nonlocal effects, we provide an overview of the basic concepts of TESHG. The TESHG process consists of three steps: (i) field enhancement at the nanogap, (ii) excitation of second-order nonlinear polarization, and (iii) radiation of second-harmonics. First, the incident laser ($E_0(\omega)$) is plasmonically enhanced at the nanogap. We define the ratio of the resulting enhanced field ($E_{gap}(\omega)$) to the incident field as the enhancement factor $K_{gap}(\omega)$:[30,31]

$$E_{gap}(\omega) = K_{gap}(\omega) E_0(\omega). \quad (1)$$

This enhanced field induces the second-order nonlinear polarization $P^{(2)}(2\omega)$:

$$P^{(2)}(2\omega) = \chi^{(2)}(2\omega; \omega, \omega) E_{gap}^2(\omega) = \chi^{(2)}(2\omega; \omega, \omega) K_{gap}^2(\omega) E_0^2(\omega), \quad (2)$$

where $\chi^{(2)}(2\omega; \omega, \omega)$ is the second-order nonlinear susceptibility. The induced $P^{(2)}(2\omega)$ then emits second harmonics ($E_{TESHG}(2\omega)$):

$$E_{TESHG}(2\omega) \propto L_{gap}(2\omega) P^{(2)}(2\omega), \quad (3)$$

where $L_{gap}(2\omega)$ is the radiation efficiency of TESHG from $P^{(2)}(2\omega)$.[31] The resultant TESHG intensity ($I_{TESHG}(2\omega)$) is given by

$$I_{TESHG}(2\omega) \propto |E_{TESHG}(2\omega)|^2 \propto \left|L_{gap}(2\omega)\right|^2 \left|\chi^{(2)}(2\omega; \omega, \omega)\right|^2 \left|K_{gap}(\omega)\right|^4 I_0^2(\omega), \quad (4)$$

where $I_0(\omega)$ is the intensity of the incident light and the relationship of $I_0(\omega) \propto |E_0(\omega)|^2$ has been applied. Note that $I_0(\omega)$ was kept constant (0.3 mW) within the wavelength range swept in this experiment. Moreover, because both incident excitation light and emitted SHG light are non-resonant with electronic transitions of gold, we can assume that the frequency dependence of $\chi^{(2)}(2\omega; \omega, \omega)$ is small.[32–34] Therefore, the overall frequency profile of $I_{TESHG}(2\omega)$ is approximated as

$$I_{TESHG}(2\omega) \propto \left|K_{gap}(\omega)\right|^4 \left|L_{gap}(2\omega)\right|^2. \quad (5)$$

This indicates that the observed TESHG responses for various tips (Figure 2 and 3) can be generally described by considering the tip dependence of local and nonlocal effects in $K_{gap}(\omega)$ and $L_{gap}(2\omega)$. To provide microscopic insights into the tip-dependent TESHG responses in wide frequency (wavelength) range, we quantitatively analyzed these two factors using FDTD method (See Supporting Information for details of the calculation procedures).

We start by modeling an STM tip as a nanosphere without a shaft[35–40] (Figure 4a) to focus on the local plasmonic effects that occur at the nanogap between the substrate and tip apexes. Figures 4b and c show the wavelength dependence of K_{gap} and L_{gap} calculated for the

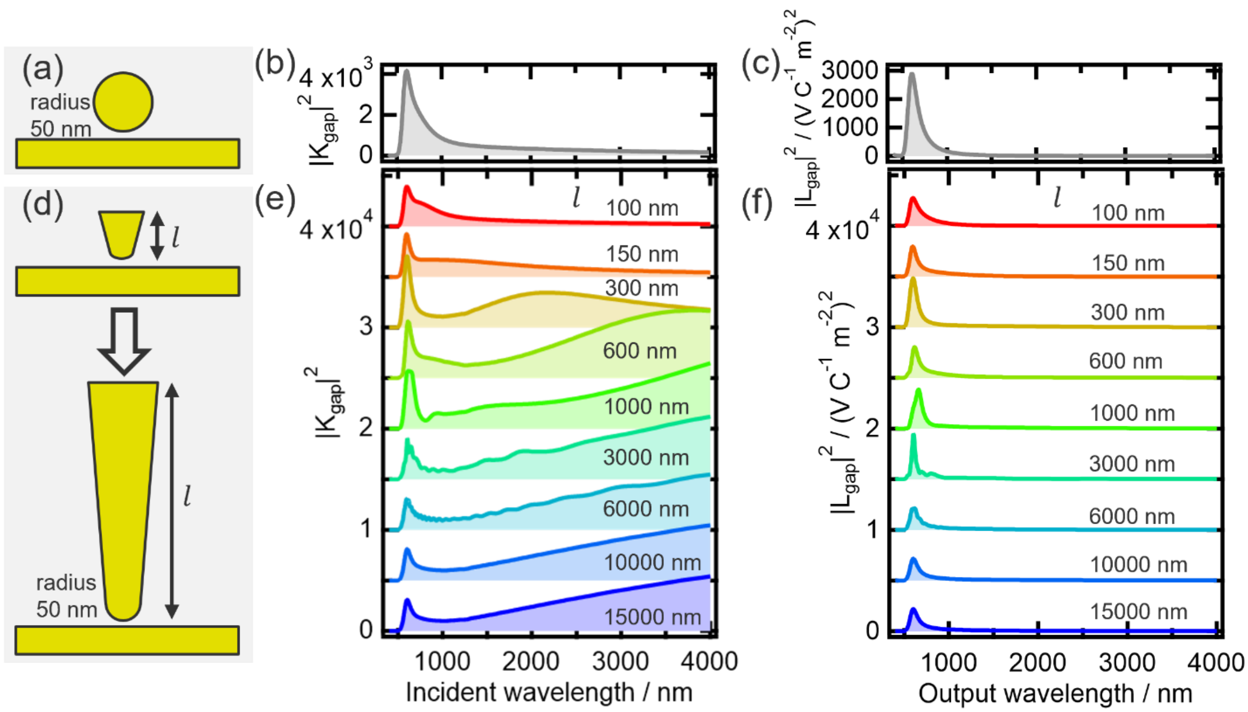

Figure 4 (a) Schematic representation of nanosphere-substrate configuration. The radius of the nanosphere is 50 nm. (b) $|K_{gap}|^2$ and (c) $|L_{gap}|^2$ spectra of the nanogap in a nanosphere-substrate system calculated through the FDTD method. (d) Schematic representation of tip-substrate configuration. A rounded cone tip with a 30° opening angle and 50 nm radius of curverture was adopted in the calculation. The tip length l was changed from 100 nm to 15000 nm. (e) and (f): Tip-length dependent (e) $|K_{gap}|^2$ and (f) $|L_{gap}|^2$ spectra of a tip-substrate nanocavity calculated through the FDTD method. The tip lengths are indicated in the figures and the tip-substrate distance d was taken as 1 nm for all these calculations.

nanosphere-substrate system, respectively. The spectra only exhibit a single band in the visible region, indicating that only visible light is enhanced in the nanosphere-substrate system. This has been proven to be a typical signature of the gap-mode plasmon excitation localized between the nanogap.[37,41–43] Conversely, both of the K_{gap} and L_{gap} values in the infrared region seem to be too small to describe the enhancement of infrared-light induced TESHG. This implies that micrometer-scale tip shafts, which were not considered in the nanosphere-substrate system, play an important role in the enhancement of the infrared region.

We then investigated the influence of macroscopic shafts of cone-shaped tips (Figure 4d). Although short tips ($l \leq 150$ nm) exhibit enhancement limited to the visible range, tips with macroscopic shafts (particularly $l \geq 600$ nm) extend the spectral range of the field enhancement to the near- and even mid-infrared region (Figure 4e). The drastic enhancement in the infrared region is a clear manifestation of the nonlocal effects caused by the tip shafts. This can be attributed to the so-called antenna effect caused by the collective oscillation of electrons over the entire tip (See Supporting Information for details).[44–47] In contrast, in the radiation process, this nonlocal effect is not pronounced. As shown in Figure 4f, efficient radiation occurs only in the visible region regardless of the tip length l. Although the tip length causes slight differences in the strength and shape of the L_{gap} spectra, the wavelength range of efficient radiation from nanocavities is predominantly determined by gap-mode plasmons.

The spectral behaviors of K_{gap} and L_{gap} in long tips are key to understand the mechanism of TESHG. The broad enhancement of incident light in the near-to-mid-infrared region (K_{gap}) and relatively narrow radiation efficiency in the visible-to-near-infrared region (L_{gap}) encompassed the excitation (1300–2000 nm) and SHG radiation (650–1000 nm) wavelength ranges in our experiments, respectively. This indicates that local and nonlocal effects jointly contribute to TESHG; the nonlocal plasmonic response over the micrometer-scale tip shafts enables the enhancement of incident infrared excitation pulses, while the local gap-mode plasmons effectively intensify the radiation of second harmonics.

As both nanometer-scale tip apexes and micrometer-scale tip shafts critically influence the TESHG process, our results suggest that controlling the geometries of these domains in tips should enable us to actively manipulate the nonlinear optical properties of the tip-substrate nanocavities. In this regard, tip tuning through varying tip sharpness (tips #1 and #2) and introducing surface roughness on the shaft (tip #3) can be regarded as first-step demonstrations of the geometrical engineering of tip-enhanced nonlinear optical processes. To examine the specific effects of such structural modulation, we again performed an FDTD simulation using the realistic tip geometries of tips #1, #2, and #3 (Figures 5a–c) obtained from their scanning electron micrographs shown in Figures 1 and 3.

The variation in the TESHG intensity induced by changing the nanometer-scale tip sharpness (tips #1 and #2) can be understood in terms of gap-mode plasmon tuning. As shown in Figures 5d and e, in the range $\lambda_{2\omega} \leq 1000$ nm, the sharper tip (tip #2) has a higher-energy gap-mode resonance; the resonance peak for tip #1 is in the experimentally scanned SHG wavelength range (blue-shaded area) while the peak for tip #2 is blue-shifted from there. This sharpness dependence of resonance energy is consistent with the previous reports on STM luminescence[48], tip-enhanced Raman scattering,[49] and theoretical calculations of plasmonic field[41,42,46] reporting that a smaller apex can support higher-energy gap-mode plasmons. Reflecting these spectral structures, significant differences in the overall wavelength dependence of the TESHG intensity emerge between the two tips (Figures 5g and h): a single broad peak structure for tip #1 and a monotonical decrease for tip #2. Notably, these behaviors qualitatively agree with the experimental results for tips #1 and #2 (Figures 2 and 3c). This demonstrates the importance of tuning the local nanometer-scale apexes on the nonlinear optical properties of tip-substrate nanocavities.

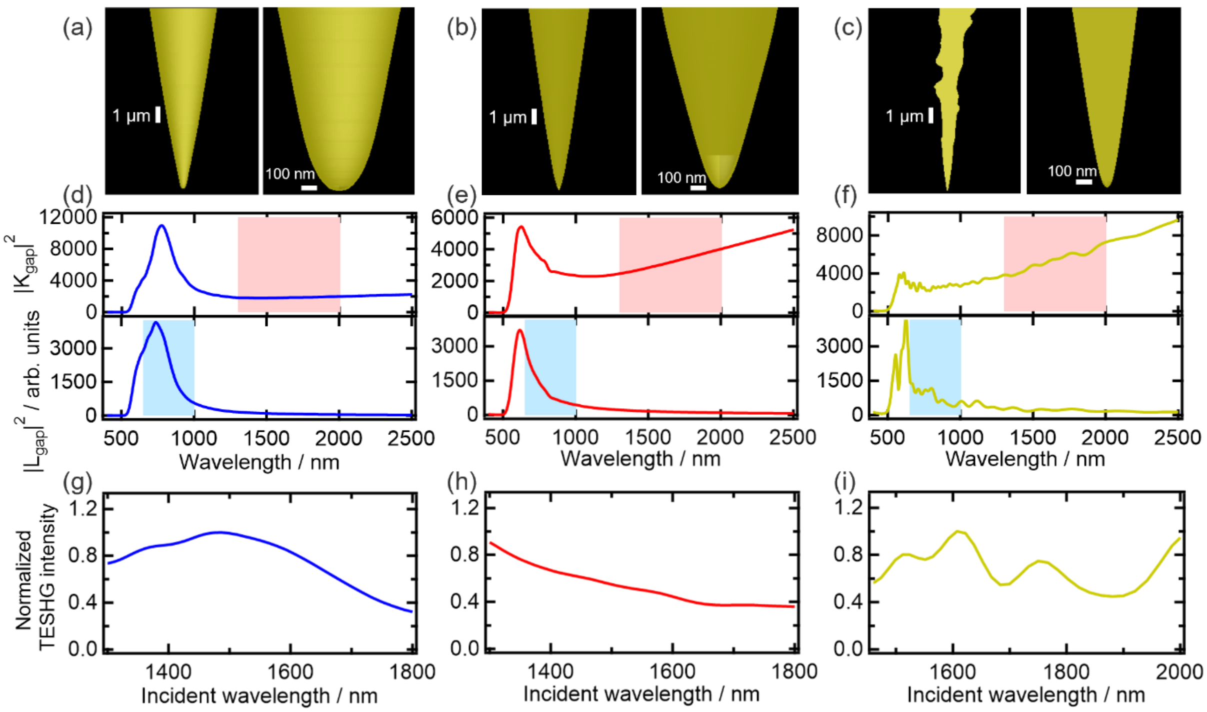

Figure 5 (a)-(c): Structures of (a) tip #1, (b) tip #2, and (c) tip #3 used in the FDTD simulation, which were depicted by tracing the outlines of the scanning electron micrographs shown in Figure 3. The scale bar lengths for left and right panels are 1μm and 100 nm, respectively. (d)-(f): $|K_{gap}|^2$ (upper panels) and $|L_{gap}|^2$ (lower panels) spectra calculated by using realisitic tip geometries for (d) tip #1, (e) tip #2, and (f) tip #3. The excitation (ω) and radiation (2ω) wavelength ranges swept in our experiment are indicated by the red and blue shaded areas, respectively. (g)-(i): The excitation wavelength–dependence of the TESHG intensity calculated by Eq. 5. (g), (h), and (i) show the results for tip #1, tip #2, and tip #3 respectively.

The introduction of surface roughness on the shaft (tip #3) has a more complicated influence. The roughness induces several irregular antenna-modes that are absent in the smooth tips, giving rise to a complex oscillatory structure in the K_{gap} and L_{gap} spectra (Figure 5f). The resultant wavelength dependence of the TESHG intensity thus exhibits an irregular shape (Figure 5i), which qualitatively captures the characteristics of the observed TESHG behavior for tip #3

(Figure 3f). This indicates that micrometer-scale processing of tip shafts can be used to drastically modulate the nonlinear optical responses at the nanogap.

The consistency between the experimental and simulated results also indicates that when exact nanometer-scale and micrometer-scale tip geometries are given, we can generally predict the plasmonic nonlinear optical properties of tip-substrate nanocavities over a wide wavelength range. This predictability allows optimization of tips by computational design for the efficient enhancement of nonlinear optical processes. More precise modulation of local and nonlocal tip geometries by nanoscale adjustments of the apex curvature and grooving patterns on the tip shafts is a key for intentionally controlling nonlinear optical properties. Such fine control of tip geometries can be achieved by exploiting more sophisticated tip processing technologies, such as focused ion beam processing.[50] Based on the present work, our forthcoming study on the interplay between theoretical modeling and high-level tip fabrication techniques will further accelerate the development of tip-enhanced nonlinear optics.

In summary, we showed that the local and nonlocal geometries of plasmonic tips have a prominent influence on the visible-to-infrared nonlinear optical responses in tip-substrate nanocavities. TESHG measurements with structurally tuned tips revealed the critical roles played by nanosized tip apexes and macroscale tip shafts in the broadband enhancement processes of nonlinear optical phenomena. These structural effects can be understood by the contributions of local gap-mode and nonlocal antenna-mode plasmons; micrometer-scale tip shafts promote the collective oscillation of electrons throughout the tip (antenna-mode), which enhances the incoming infrared field, while local gap-mode plasmons intensify the radiation of second harmonics in the visible domain. We verified that the concerted contributions of these local and nonlocal effects are the origin of the enhancement of nonlinear optical phenomena ranging in visible-to-infrared broadband wavelength region. Based on this understanding of the tip-enhancement mechanism, our experimental results for the differently structured tips were successfully described. This will serve as a firm basis for more precise nano- and micrometer-scale tip engineering to finely manipulate nonlinear optical processes at the nanogap.

ASSOCIATED CONTENT

Supporting Information.

The Supporting Information is available free of charge.

Methods, threshold of excitation intensity, and discussion on the non-local effects of tip shafts (PDF)

AUTHOR INFORMATION

Corresponding Authors

Atsunori Sakurai — Department of Materials Molecular Science, Institute for Molecular Science (IMS), Okazaki, Aichi 444-8585, Japan; The Graduate University for Advanced Studies, SOKENDAI, Hayama, Kanagawa, 240-0193, Japan; orcid.org/0000-0002-4410-7518; Email: asakurai@ims.ac.jp

Toshiki Sugimoto — Department of Materials Molecular Science, Institute for Molecular Science (IMS), Okazaki, Aichi 444-8585, Japan; The Graduate University for Advanced Studies, SOKENDAI, Hayama, Kanagawa, 240-0193, Japan; Precursory Research for Embryonic Science and Technology (PRESTO), Japan Science and Technology Agency (JST), 4-1-8 Honcho, Kawaguchi, Saitama 332-0012, Japan; orcid.org/0000-0003-3453-6009; Email: toshiki-sugimoto@ims.ac.jp

Authors

Shota Takahashi — Department of Materials Molecular Science, Institute for Molecular Science (IMS), Okazaki, Aichi 444-8585, Japan; orcid.org/0000-0002-7191-5051

Tatsuto Mochizuki — Department of Materials Molecular Science, Institute for Molecular Science (IMS), Okazaki, Aichi 444-8585, Japan; The Graduate University for Advanced Studies, SOKENDAI, Hayama, Kanagawa, 240-0193, Japan; orcid.org/0000-0002-8587-3585

Notes

The authors declare no competing financial interest.

ACKNOWLEDGMENT

The authors would like to thank Prof. Maki Kawai and Prof. Toshihiko Yokoyama for their great support in starting up this project, Ekuko Nohno and Dr. Hikaru Saito for developing the fabrication method of the Au tips at an early stage of the project, and the Equipment Development Center of Institute for Molecular Science for technical assistance. We also thank Hiroko Yoshino and Prof. Takashi Kumagai for helpful advice on STM operation and tip-forming, and Prof. Akihito Ishizaki for allowing us to use a computer cluster of his group. This work was supported by JST-PRESTO JPMJPR1907; JST-CREST JPMJCR22L2; JSPS KAKENHI Grant-in-Aid for Scientific Research (A), No. 19H00865, and 22H00296; Grant-in-Aid for Research Activity Start-up No. 19K23640; Grant-in-Aid for Early-Career Scientists, No. 20K15236; Grant-in-Aid for JSPS Fellows No. 22J01438; CASIO SCIENCE PROMOTION FOUNDATION No. 38-06; and Research Foundation for Opto-Science and Technology.

REFERENCES

(1) Chen, X.; Hu, D.; Mescall, R.; You, G.; Basov, D. N.; Dai, Q.; Liu, M. Modern Scattering-Type Scanning Near-Field Optical Microscopy for Advanced Material Research. *Adv. Mater.* **2019**, *31* (24), 1804774. https://doi.org/10.1002/adma.201804774.

(2) Pienpinijtham, P.; Kitahama, Y.; Ozaki, Y. Progress of Tip-Enhanced Raman Scattering for the Last Two Decades and Its Challenges in Very Recent Years. *Nanoscale* **2022**, *14* (14), 5265–5288. https://doi.org/10.1039/D2NR00274D.

(3) Lee, H.; Lee, D. Y.; Kang, M. G.; Koo, Y.; Kim, T.; Park, K.-D. Tip-Enhanced Photoluminescence Nano-Spectroscopy and Nano-Imaging. *Nanophotonics 9* (10), 3089–3110.

(4) Kumagai, T. Sub-Molecular Photoluminescence. *Nat. Photonics* **2020**, *14* (11), 653–655. https://doi.org/10.1038/s41566-020-00706-6.

(5) Wang, C.-F.; El-Khoury, P. Z. Multimodal (Non)Linear Optical Nanoimaging and Nanospectroscopy. *J. Phys. Chem. Lett.* **2022**, *13* (31), 7350–7354. https://doi.org/10.1021/acs.jpclett.2c01993.

(6) Smolyaninov, I. I.; Zayats, A. V.; Davis, C. C. Near-Field Second Harmonic Generation from a Rough Metal Surface. *Phys. Rev. B* **1997**, *56* (15), 9290–9293. https://doi.org/10.1103/PhysRevB.56.9290.

(7) Schaller, R. D.; Johnson, J. C.; Wilson, K. R.; Lee, L. F.; Haber, L. H.; Saykally, R. J. Nonlinear Chemical Imaging Nanomicroscopy: From Second and Third Harmonic Generation to Multiplex (Broad-Bandwidth) Sum Frequency Generation Near-Field Scanning Optical Microscopy. *J. Phys. Chem. B* **2002**, *106* (20), 5143–5154. https://doi.org/10.1021/jp0144653.

(8) Mahieu-Williame, L.; Grésillon, S.; Cuniot-Ponsard, M.; Boccara, C. Second Harmonic Generation in the near Field and Far Field: A Sensitive Tool to Probe Crystalline Homogeneity. *J. Appl. Phys.* **2007**, *101* (8), 083111. https://doi.org/10.1063/1.2719278.

(9) Neacsu, C. C.; van Aken, B. B.; Fiebig, M.; Raschke, M. B. Second-Harmonic near-Field Imaging of Ferroelectric Domain Structure of $YMnO_3$. *Phys. Rev. B* **2009**, *79* (10), 100107. https://doi.org/10.1103/PhysRevB.79.100107.

(10) Park, K.-D.; Raschke, M. B. Polarization Control with Plasmonic Antenna Tips: A Universal Approach to Optical Nanocrystallography and Vector-Field Imaging. *Nano Lett.* **2018**, *18* (5), 2912–2917. https://doi.org/10.1021/acs.nanolett.8b00108.

(11) Wang, C.-F.; El-Khoury, P. Z. Multimodal Tip-Enhanced Nonlinear Optical Nanoimaging of Plasmonic Silver Nanocubes. *J. Phys. Chem. Lett.* **2021**, *12* (44), 10761–10765. https://doi.org/10.1021/acs.jpclett.1c03196.

(12) Yao, K.; Zhang, S.; Yanev, E.; McCreary, K.; Chuang, H.-J.; Rosenberger, M. R.; Darlington, T.; Krayev, A.; Jonker, B. T.; Hone, J. C.; Basov, D. n.; Schuck, P. J. Nanoscale Optical Imaging of 2D Semiconductor Stacking Orders by Exciton-Enhanced Second Harmonic Generation. *Adv. Opt. Mater.* **2022**, *10* (12), 2200085. https://doi.org/10.1002/adom.202200085.

(13) Ichimura, T.; Hayazawa, N.; Hashimoto, M.; Inouye, Y.; Kawata, S. Tip-Enhanced Coherent Anti-Stokes Raman Scattering for Vibrational Nanoimaging. *Phys. Rev. Lett.* **2004**, *92* (22), 220801. https://doi.org/10.1103/PhysRevLett.92.220801.

(14) Ichimura, T.; Hayazawa, N.; Hashimoto, M.; Inouye, Y.; Kawata, S. Application of Tip-Enhanced Microscopy for Nonlinear Raman Spectroscopy. *Appl. Phys. Lett.* **2004**, *84* (10), 1768–1770. https://doi.org/10.1063/1.1647277.

(15) Furusawa, K.; Hayazawa, N.; Catalan, F. C.; Okamoto, T.; Kawata, S. Tip-Enhanced Broadband CARS Spectroscopy and Imaging Using a Photonic Crystal Fiber Based Broadband Light Source. *J. Raman Spectrosc.* **2012**, *43* (5), 656–661. https://doi.org/10.1002/jrs.3151.

(16) Lin, J.; Zi Jian Er, K.; Zheng, W.; Huang, Z. Radially Polarized Tip-Enhanced near-Field Coherent Anti-Stokes Raman Scattering Microscopy for Vibrational Nano-Imaging. *Appl. Phys. Lett.* **2013**, *103* (8), 083705. https://doi.org/10.1063/1.4819236.

(17) Kravtsov, V.; Ulbricht, R.; Atkin, J. M.; Raschke, M. B. Plasmonic Nanofocused Four-Wave Mixing for Femtosecond near-Field Imaging. *Nat. Nanotechnol.* **2016**, *11* (5), 459–464. https://doi.org/10.1038/nnano.2015.336.

(18) Wang, C.-F.; El-Khoury, P. Z. Imaging Plasmons with Sub-2 Nm Spatial Resolution via Tip-Enhanced Four-Wave Mixing. *J. Phys. Chem. Lett.* **2021**, *12* (14), 3535–3539. https://doi.org/10.1021/acs.jpclett.1c00763.

(19) Aouani, H.; Navarro-Cia, M.; Rahmani, M.; Sidiropoulos, T. P. H.; Hong, M.; Oulton, R. F.; Maier, S. A. Multiresonant Broadband Optical Antennas As Efficient Tunable Nanosources of Second Harmonic Light. *Nano Lett.* **2012**, *12* (9), 4997–5002. https://doi.org/10.1021/nl302665m.

(20) Celebrano, M.; Wu, X.; Baselli, M.; Großmann, S.; Biagioni, P.; Locatelli, A.; De Angelis, C.; Cerullo, G.; Osellame, R.; Hecht, B.; Duò, L.; Ciccacci, F.; Finazzi, M. Mode Matching in

Multiresonant Plasmonic Nanoantennas for Enhanced Second Harmonic Generation. *Nat. Nanotechnol.* **2015**, *10* (5), 412–417. https://doi.org/10.1038/nnano.2015.69.

(21) Zhang, N.; Ji, Z.; Cheney, A. R.; Song, H.; Ji, D.; Zeng, X.; Chen, B.; Zhang, T.; Cartwright, A. N.; Shi, K.; Gan, Q. Ultra-Broadband Enhancement of Nonlinear Optical Processes from Randomly Patterned Super Absorbing Metasurfaces. *Sci. Rep.* **2017**, *7* (1), 4346. https://doi.org/10.1038/s41598-017-04688-4.

(22) Yang, B.; Kazuma, E.; Yokota, Y.; Kim, Y. Fabrication of Sharp Gold Tips by Three-Electrode Electrochemical Etching with High Controllability and Reproducibility. *J. Phys. Chem. C* **2018**, *122* (29), 16950–16955. https://doi.org/10.1021/acs.jpcc.8b04078.

(23) Pyykko, P.; Desclaux, J. P. Relativity and the Periodic System of Elements. *Acc. Chem. Res.* **1979**, *12* (8), 276–281. https://doi.org/10.1021/ar50140a002.

(24) Dougherty, D. B.; Maksymovych, P.; Lee, J.; Feng, M.; Petek, H.; Yates, J. T. Tunneling Spectroscopy of Stark-Shifted Image Potential States on Cu and Au Surfaces. *Phys. Rev. B* **2007**, *76* (12), 125428. https://doi.org/10.1103/PhysRevB.76.125428.

(25) Lin, C. L.; Lu, S. M.; Su, W. B.; Shih, H. T.; Wu, B. F.; Yao, Y. D.; Chang, C. S.; Tsong, T. T. Manifestation of Work Function Difference in High Order Gundlach Oscillation. *Phys. Rev. Lett.* **2007**, *99* (21), 216103. https://doi.org/10.1103/PhysRevLett.99.216103.

(26) Su, W.-B.; Lin, C.-L.; Chan, W.-Y.; Lu, S.-M.; Chang, C.-S. Field Enhancement Factors and Self-Focus Functions Manifesting in Field Emission Resonances in Scanning Tunneling Microscopy. *Nanotechnology* **2016**, *27* (17), 175705. https://doi.org/10.1088/0957-4484/27/17/175705.

(27) Rosławska, A.; Merino, P.; Grewal, A.; Leon, C. C.; Kuhnke, K.; Kern, K. Atomic-Scale Structural Fluctuations of a Plasmonic Cavity. *Nano Lett.* **2021**, *21* (17), 7221–7227. https://doi.org/10.1021/acs.nanolett.1c02207.

(28) Klingsporn, J. M.; Sonntag, M. D.; Seideman, T.; Van Duyne, R. P. Tip-Enhanced Raman Spectroscopy with Picosecond Pulses. *J. Phys. Chem. Lett.* **2014**, *5* (1), 106–110. https://doi.org/10.1021/jz4024404.

(29) Pozzi, E. A.; Sonntag, M. D.; Jiang, N.; Chiang, N.; Seideman, T.; Hersam, M. C.; Van Duyne, R. P. Ultrahigh Vacuum Tip-Enhanced Raman Spectroscopy with Picosecond Excitation. *J. Phys. Chem. Lett.* **2014**, *5* (15), 2657–2661. https://doi.org/10.1021/jz501239z.

(30) Eric C. Le Ru, G. E. *Principles of Surface-Enhanced Raman Spectroscopy and Related Plasmonic Effects*; Elsevier, 2009.

(31) Lambert, A. G.; Davies, P. B.; Neivandt, D. J. Implementing the Theory of Sum Frequency Generation Vibrational Spectroscopy: A Tutorial Review. *Appl. Spectrosc. Rev.* **2005**, *40* (2), 103–145. https://doi.org/10.1081/ASR-200038326.

(32) Dalstein, L.; Revel, A.; Humbert, C.; Busson, B. Nonlinear Optical Response of a Gold Surface in the Visible Range: A Study by Two-Color Sum-Frequency Generation Spectroscopy. I. Experimental Determination. *J. Chem. Phys.* **2018**, *148* (13), 134701. https://doi.org/10.1063/1.5021553.

(33) Busson, B.; Dalstein, L. Nonlinear Optical Response of a Gold Surface in the Visible Range: A Study by Two-Color Sum-Frequency Generation Spectroscopy. II. Model for Metal

Nonlinear Susceptibility. *J. Chem. Phys.* **2018**, *149* (3), 034701. https://doi.org/10.1063/1.5027154.

(34) Busson, B.; Dalstein, L. Nonlinear Optical Response of a Gold Surface in the Visible Range: A Study by Two-Color Sum-Frequency Generation Spectroscopy. III. Simulations of the Experimental SFG Intensities. *J. Chem. Phys.* **2018**, *149* (15), 154701. https://doi.org/10.1063/1.5047098.

(35) Martín-Jiménez, A.; Fernández-Domínguez, A. I.; Lauwaet, K.; Granados, D.; Miranda, R.; García-Vidal, F. J.; Otero, R. Unveiling the Radiative Local Density of Optical States of a Plasmonic Nanocavity by STM. *Nat. Commun.* **2020**, *11* (1), 1021. https://doi.org/10.1038/s41467-020-14827-7.

(36) Heilman, A. L.; Hermann, R. J.; Gordon, M. J. Direct Detection of Gap Mode Plasmon Resonances Using Attenuated Total Reflection-Based Tip-Enhanced near-Field Optical Microscopy. *J. Opt.* **2020**, *22* (9), 095001. https://doi.org/10.1088/2040-8986/aba47e.

(37) Porto, J. A.; Johansson, P.; Apell, S. P.; López-Ríos, T. Resonance Shift Effects in Apertureless Scanning Near-Field Optical Microscopy. *Phys. Rev. B* **2003**, *67* (8), 085409. https://doi.org/10.1103/PhysRevB.67.085409.

(38) Krug, J. T.; Sánchez, E. J.; Xie, X. S. Design of Near-Field Optical Probes with Optimal Field Enhancement by Finite Difference Time Domain Electromagnetic Simulation. *J. Chem. Phys.* **2002**, *116* (24), 10895–10901. https://doi.org/10.1063/1.1479723.

(39) Madrazo, A.; Nieto-Vesperinas, M.; García, N. Exact Calculation of Maxwell Equations for a Tip-Metallic Interface Configuration: Application to Atomic Resolution by Photon Emission. *Phys. Rev. B* **1996**, *53* (7), 3654–3657. https://doi.org/10.1103/PhysRevB.53.3654.

(40) Esteban, R.; Vogelgesang, R.; Kern, K. Tip-Substrate Interaction in Optical near-Field Microscopy. *Phys. Rev. B* **2007**, *75* (19), 195410. https://doi.org/10.1103/PhysRevB.75.195410.

(41) Li, G.; Gao, M.; Xu, X.; Li, Y.; Meng, L.; Yang, Z. Plasmonic Enhancement and Directional Emission for Side-Illumination Tip-Enhanced Spectroscopy. *Opt. Commun.* **2019**, *442*, 50–55. https://doi.org/10.1016/j.optcom.2019.02.067.

(42) Wei, Y.; Pei, H.; Sun, D.; Duan, S.; Tian, G. Numerical Investigations on the Electromagnetic Enhancement Effect to Tip-Enhanced Raman Scattering and Fluorescence Processes. *J. Phys.: Condens. Matter* **2019**, *31* (23), 235301. https://doi.org/10.1088/1361-648X/ab0b9d.

(43) Futamata, M.; Ishikura, M.; Iida, C.; Handa, S. The Critical Importance of Gap Modes in Surface Enhanced Raman Scattering. *Faraday Discuss.* **2015**, *178* (0), 203–220. https://doi.org/10.1039/C4FD00188E.

(44) Huth, F.; Chuvilin, A.; Schnell, M.; Amenabar, I.; Krutokhvostov, R.; Lopatin, S.; Hillenbrand, R. Resonant Antenna Probes for Tip-Enhanced Infrared Near-Field Microscopy. *Nano Lett.* **2013**, *13* (3), 1065–1072. https://doi.org/10.1021/nl304289g.

(45) Mastel, S.; Lundeberg, M. B.; Alonso-González, P.; Gao, Y.; Watanabe, K.; Taniguchi, T.; Hone, J.; Koppens, F. H. L.; Nikitin, A. Y.; Hillenbrand, R. Terahertz Nanofocusing with

Cantilevered Terahertz-Resonant Antenna Tips. *Nano Lett.* **2017**, *17* (11), 6526–6533. https://doi.org/10.1021/acs.nanolett.7b01924.

(46) Hermann, R. J.; Gordon, M. J. Quantitative Comparison of Plasmon Resonances and Field Enhancements of Near-Field Optical Antennae Using FDTD Simulations. *Opt. Express* **2018**, *26* (21), 27668–27682. https://doi.org/10.1364/OE.26.027668.

(47) Zhang, W.; Cui, X.; Martin, O. J. F. Local Field Enhancement of an Infinite Conical Metal Tip Illuminated by a Focused Beam. *J. Raman Spectrosc.* **2009**, *40* (10), 1338–1342. https://doi.org/10.1002/jrs.2439.

(48) Boyle, M. G.; Mitra, J.; Dawson, P. Infrared Emission from Tunneling Electrons: The End of the Rainbow in Scanning Tunneling Microscopy. *Appl. Phys. Lett.* **2009**, *94* (23), 233118. https://doi.org/10.1063/1.3154563.

(49) Yokota, Y.; Hong, M.; Hayazawa, N.; Yang, B.; Kazuma, E.; Kim, Y. Self-Consistent Tip Conditioning for Tip-Enhanced Raman Spectroscopy in an Ambient Environment. *J. Phys. Chem. C* **2020**, *124* (42), 23243–23252. https://doi.org/10.1021/acs.jpcc.0c07579.

(50) Böckmann, H.; Liu, S.; Müller, M.; Hammud, A.; Wolf, M.; Kumagai, T. Near-Field Manipulation in a Scanning Tunneling Microscope Junction with Plasmonic Fabry-Pérot Tips. *Nano Lett.* **2019**, *19* (6), 3597–3602. https://doi.org/10.1021/acs.nanolett.9b00558.

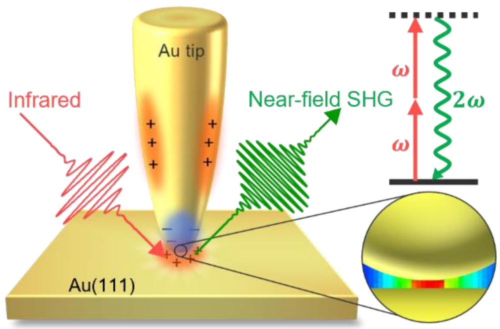

For Table of Contents Only